Available online at www.sciencedirect.com
SCIENCE DIRECT
Tectonophysics 417 (2006) 325–335
TECTONOPHYSICS
www.elsevier.com/locate/tecto

Estimates of heat flow from Cenozoic seafloor using global depth and age data

Meng Wei *, David Sandwell

Scripps Institution of Oceanography, La Jolla, CA 92093-0225, United States

Received 31 October 2005; received in revised form 27 January 2006; accepted 1 February 2006
Available online 23 March 2006

Abstract

The total heat output of the Earth constrains models of mantle and core dynamics. Previously published estimates (42–44 TW) have recently been questioned because the measured conductive heat flow on young oceanic lithosphere is about a factor of 2 less than the expected heat flow based on half-space cooling models. Taking the conductive ocean heat flow values at face value reduces the global heat flow from 44 to 31 TW, which has major implications for geodynamics and Earth history. To help resolve this issue, we develop a new method of estimating total oceanic heat flow from depth and age data. The overall elevation of the global ridge system, relative to the deep ocean basins, provides an independent estimate of the total heat content of the lithosphere. Heat flow is proportional to the measured subsidence rate times the heat capacity divided by the thermal expansion coefficient. The largest uncertainty in this method is due to uncertainties in the thermal expansion coefficient and heat capacity. Scalar subsidence rate is computed from gradients of depth and age grids. The method cannot be applied over very young seafloor (<3 Ma) where age gradient is discontinuous and the assumption of isostasy is invalid. Between 3 and 66 Ma, the new estimates are in agreement with half-space cooling model. Our model-independent estimate of the total heat output of Cenozoic seafloor is 18.6 to 20.5 TW, which leads to a global output of 42 to 44 TW in agreement with previous studies.

Keywords: Oceanic heat flow; Global heat budget; Subsidence rate

1. Introduction

The total heat output of the Earth is comprised of heat flow from the core, radiogenic heat production in the mantle, secular cooling of the Earth, and radiogenic heat production in the continental crust. While the magnitude of the individual components is highly uncertain, the total surface heat output has been estimated at 42–44 TW (Sclater et al., 1980; Pollack et al., 1993). Recently this estimate has been questioned (Hofmeister and Criss, 2005) mainly because the measured conductive heat flow on young oceanic lithosphere is about a factor of 2 less than the total heat flow based on cooling models. Taking conductive ocean heat flow measurements at face value leads to a global heat output of only 31 TW. A reduction of this magnitude has important implications for heat flow across the core/mantle boundary, which is believed to drive mantle plumes. Moreover Hofmeister and Criss (2005) argue that this lower value of global heat flux is more consistent with the isotope chemistry and cooling history of the Earth.

The origin of 13 TW of this difference in global heat output is related to how one assesses heat flow over Cenozoic oceanic lithosphere (0–66 Ma). Lithospheric cooling models, based primarily on the increase in

* Corresponding author.
E-mail address: mwei@ucsd.edu (M. Wei).

0040-1951/$ - see front matter © 2006 Elsevier B.V. All rights reserved.
doi:10.1016/j.tecto.2006.02.004

seafloor depth with age, but also on conductive surface heat flow over older lithosphere (>40 Ma) predict high heat flow values at ridges and on young ridge flanks (McKenzie, 1967; Davis and Lister, 1974; Parsons and Sclater, 1977; Stein and Stein, 1992). Moreover, in the case of a one-dimensional approximation to the heat conduction equation, the models have an infinite heat flow at zero age. While the integrated heat flow for these models is non-singular (Oldenburg, 1975) it is nevertheless a factor of 2 greater than the integrated measured heat flow. There are two ways to understand this discrepancy.

A) The total heat flow out of the top of the plate matches the predictions of the cooling models but conductive heat flow probes cannot "see" the total value because much of the heat is advected by hydrothermal circulation (Lister, 1972; Williams et al., 1974; Anderson and Hobart, 1976; Sleep and Wolery, 1978). In this case, the discrepancy between the measured (conductive) and total lithospheric heat flow provides an estimate of advective heat loss (Stein and Stein, 1994).
B) The total heat flow out of the top of the plate is nearly equal to the measured conductive heat flow. Hofmeister and Criss (2005) provide a number of theoretical and observational arguments in favor of this case. They claim that that hydrothermal circulation cannot cause the huge discrepancy because the MOR magma system is too small and hydrothermal systems are weak movers of heat.

In this paper we use the observed subsidence of the spreading ridges and physically realistic bounds on thermal expansion coefficient and heat capacity to resolve this issue. As shown in previous studies, elevation of ridges reflects total heat content of lithosphere (Parsons and McKenzie, 1978; Doin and Fleitout, 1996). Therefore, the scalar subsidence rate is a direct measure of the difference between surface heat flow and heat flow into the base of the plate (Sandwell and Poehls, 1980). We re-derive this direct relationship between subsidence rate and lithospheric heat loss by using conservation of energy and local isostasy. The relationship does not rely on a particular cooling model and is therefore independent of the thermal conductivity of the lithosphere. Using gridded topography and age data, we estimate total surface heat flow and show it is consistent with the half-space cooling (HSC) model between ages of 3 and 66 Ma. Note that we make our comparisons with the HSC model rather than the more widely accepted plate model because the two models predict the same depth versus age relation between 0 and 70 Ma and the same heat flow versus age relation between 0 and 120 Ma (Parsons and Sclater, 1977). Our new method of estimating total heat flow fails to provide reliable estimates directly at the ridges for two reasons. First the assumption of local isostasy is not valid because ridge-axis topography is partly supported by dynamics and flexure (Cochran, 1979). Second, the seafloor subsidence rate near the ridge axis (<2 Ma) is anomalously low due to the rapid quenching of the crust by hydrothermal circulation (Cochran and Buck, 2001). Overall the results are in agreement with a global heat output of 42–44 TW (Sclater et al., 1980; Pollack et al., 1993).

2. Theory

The theory is based on energy conservation, thermal contraction, and isostasy and does not rely on any particular heat transfer model (Parsons and McKenzie, 1978). Assuming steady-state spreading and no internal heat generation, the conservation of energy is given by the time independent equation of heat transport where horizontal advection is balanced by the divergence of the heat flux.

$$\rho_m C_p \mathbf{v}\cdot\nabla T = \nabla\cdot\mathbf{q} \tag{1}$$

where T is temperature, $\mathbf{q}$ is the heat flux vector, ρ_m the density, C_p the specific heat, and $\mathbf{v}$ is the horizontal velocity of the plate. We use the principles of thermal contraction and isostasy to determine the increase in seafloor depth with increasing age $d(t)$. A reduction in temperature will cause an increase in density ρ as

$$\rho(T) = \rho_m[1-\alpha(T-T_m)] \tag{2}$$

where ρ_m is the density of the lithosphere at a temperature of T_m and α is the coefficient of thermal expansion. For thermal isostasy, the seafloor depth depends on the integrated temperature as

$$d(t) = \frac{-\alpha\rho_m}{\rho_m-\rho_w}\int_d^L (T-T_m)dz \tag{3}$$

where ρ_m is the density of seawater and L is the depth to the bottom of the thermal boundary layer and also the depth of compensation. Taking the gradient of both sides of Eq. (3) and then the dot product with the plate velocity results in

$$\mathbf{v}\cdot\nabla d(t) = \frac{-\alpha\rho_m}{\rho_m-\rho_w}\int_d^L \mathbf{v}\cdot\nabla T dz \tag{4}$$

Next we use conservation of energy (Eq. (1)) to re-write Eq. (4) as

$$\mathbf{v}\cdot\nabla d = \frac{-\alpha}{(\rho_m-\rho_w)C_p}\int_d^L \nabla\cdot\mathbf{q}\,dz \tag{5}$$

Finally by neglecting lateral heat transport on the right side of Eq. (5) and integrating, we arrive at

$$\int_d^L \frac{\partial}{\partial z}q(z)dz = q(L)-q(d) = q_b-q_s \tag{6}$$

where q_s and q_b are the surface heat flow and basal heat flow, respectively. Substitution of Eq. (6) into Eq. (5), it gives

$$\mathbf{v}\cdot\nabla d = \frac{-\alpha}{(\rho_m-\rho_w)C_p}(q_b-q_s) \tag{7}$$

This equation relates the scalar subsidence rate to the difference between the surface and basal heat flow and it depends only on the thermal expansion coefficient, the heat capacity and the densities of mantle and seawater. Given a grid of seafloor age $A(\mathbf{x})$ (Mueller et al., 1997), the local fossil spreading velocity is $\mathbf{v} = \frac{\nabla A}{\nabla A\cdot\nabla A}$. The final expression becomes

$$q_s = \frac{(\rho_m-\rho_w)C_p}{\alpha}\frac{\nabla A\cdot\nabla d}{\nabla A\cdot\nabla A} + q_b \tag{8}$$

Eq. (8) provides a way to calculate surface heat flow based on depth and age data sets as well as an estimate of basal heat flow. Note that the result is independent of thermal conductivity and its possible depth variations so the objection of Hofmeister and Criss (2005) that the temperature variations in thermal conductivity have been overlooked is now irrelevant.

While the surface heat flow estimate is independent of the vertical heat transport mechanism, it does depend on two unknown factors. First one must have an estimate of the basal heat flow, although we show below that this is not a major contribution to the integrated heat output of Cenozoic seafloor. Second one must have an estimate of the factor $(\rho_m-\rho_w)C_p/\alpha$. It would be circular reasoning to adopt values of thermal expansion coefficient and heat capacity based on modeling depth and heat flow versus age data (e.g., from Parsons and Sclater, 1977). Therefore, we must use parameter values developed independently from experimental data. As discussed in Doin and Fleitout (1996), these parameters are temperature and pressure dependent. However, Doin and Fleitout (1996) demonstrate that using temperature-averaged values provides a good approximation to the numerically integrated depth and heat-flow models which use the full temperature dependence. Doin and Fleitout (1996) use data from Kajiyoshi (1986) to compute temperature-averaged values of heat capacity and thermal expansion coefficient. They arrive at the following values that we will initially adopt for our analysis: $\alpha = 3.85\times10^{-5}$ °C^{-1}; $C_p = 1124$ J kg^{-1} °C^{-1}; $\rho_m = 3330$ kg m^{-3}; $\rho_w = 1025$ kg m^{-3}. Uncertainties in our estimates of total heat flow based on subsidence rate will depend in a first-order way on the values of these parameters and we discuss possible physical bounds on their values.

3. Mid-Atlantic ridge

The theory is first applied at Mid-Atlantic ridge to illustrate the strengths and weaknesses of the method. The result is shown in Fig. 1 where we have plotted the surface heat flow minus the basal heat flow out to an age of 66 Ma using thermal parameters and densities provided above. Over Cenozoic seafloor, the basal heat flow is believed to about 38 mW m^{-2} (Doin and Fleitout, 1996) and therefore is a minor component of the surface heat flow. We initially fix this contribution to a value of 38 mW m^{-2} but later adjust the basal heat flow to match conductive heat flow on seafloor older than 40 Ma. Most depth versus age analyses requires sediment-corrected depth before comparisons with models (Renkin and Sclater, 1988). We have not applied this correction because sediments are generally thin on young seafloor and we are interested in the depth gradient, which is independent of sediment thickness as long as the sediments are locally uniform thickness. However, if the thickness of the sediments increases systematically with age along age corridors, we will underestimate the subsidence rate and thus the total heat flow.

There are two practical problems that should be considered when computing the scalar subsidence rate $\frac{\nabla d\cdot\nabla A}{\nabla A\cdot\nabla A}$. First the age gradient ∇A should not be computed across ridges or transform faults because the denominator can go to zero in this case. Second $\frac{\partial d}{\partial t}$ can have the wrong sign in areas where there is an axial valley. The axial valley is not in isostatic equilibrium and it should not be included in the analysis. To solve these two problems, we omit seafloor younger than 0.5 Ma from the analysis and additionally mask seafloor within a 20 km distance of the ridge/transform plate boundary. The masked area is shown as a grey area in Fig. 1. We also find that raw computation of data on a 0.1° grid leads to large oscillations in the scalar subsidence rate. This is caused by two effects, short

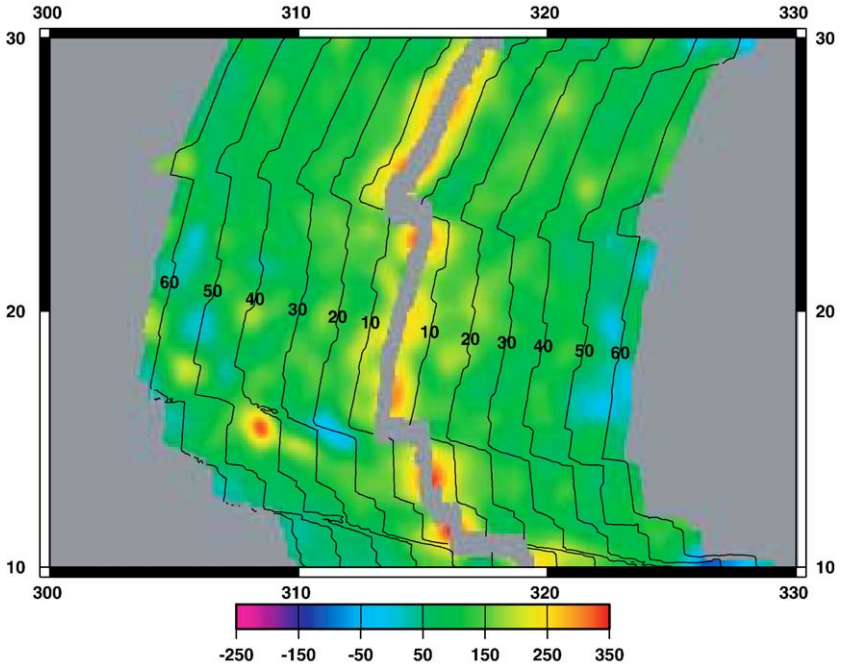

Fig. 1. Surface heat flow based on Eq. (8) using depths from a 2-min global grid (Smith and Sandwell, 1997) and ages from a global grid at 0.1° spacing (Mueller et al., 1997). A constant heat flow of 38 mW m^{-2} was added to the estimated heat flow to account for the unobserved basal heat input Doin and Fleitout (1996). Heat flow is highest on young seafloor, >250 mW m^{-2}, and decreases systematically with age out to 66 Ma. Spatial variations in heat flow could be either be due to Airy-compensated topography which produces depth gradients at scales greater than the flexural wavelength (~300 km) or perhaps real variation in surface or basal heat flow.

wavelength topography and sharp variations in the age gradient due to fracture zones and other processes. To suppress these noise processes, we smooth the scalar subsidence rate with a 2-D Gaussian filter with a 0.5 gain at a wavelength of 265 km. This filter has no effect on the average of the heat flow over age bins (Fig. 2), however the smoothing provides a realistic heat flow map as shown in Fig. 1.

To compare these heat flow estimates with lithospheric cooling models, we average the surface minus basal heat flow into 3 Ma age bins (Fig. 2, bottom). The first age bin (0.5–3.5 Ma) is sometimes partly masked over the youngest seafloor so estimates may be biased low but at greater ages we believe these estimates of heat flow are reliable. The uncertainty in each bin is the square root of the variance divided by the number of linearly independent measurements which depends on the band-width of the low-pass filter. The statistical uncertainties are quite small because the depth versus age relation is well behaved. However, these statistical uncertainties do not reflect the actual uncertainty in the heat flow estimates because, as discussed above, the uncertainties in our knowledge of the temperature-averaged thermal expansion coefficient and heat capacity are larger. Our surface heat-flow versus age estimates is in basic agreement with the theoretical curve $q = 480/\sqrt{t}$, but only after adding a basal heat flow of 38 mW m^{-2} (Doin and Fleitout, 1996). We refine this estimate of basal heat flux for the global analysis below. The important conclusion is that the estimated heat flow is significantly greater than the average of the conductive heat flow measurements. Even without this largely unknown basal heat flow contribution, the total heat flow estimates are more than 200 mW m^{-2} on 5 Ma seafloor.

In addition to estimating the total heat flow versus age we also calculate depth versus age (Fig. 2, top). Depth–age estimates are consistent with the model $d = 2500 + 350\sqrt{t}$ (Parsons and Sclater, 1977) although we find the observed depth is systematically too shallow at older ages. This could be due to neglecting the sediment correction or including areas that are anomalously shallow because of crustal thickening (Hillier and Watts, 2005).

4. Global analysis

The same analysis was performed on global depth and age data to estimate the Cenozoic heat output of the Earth. A global map of surface heat flow is shown in

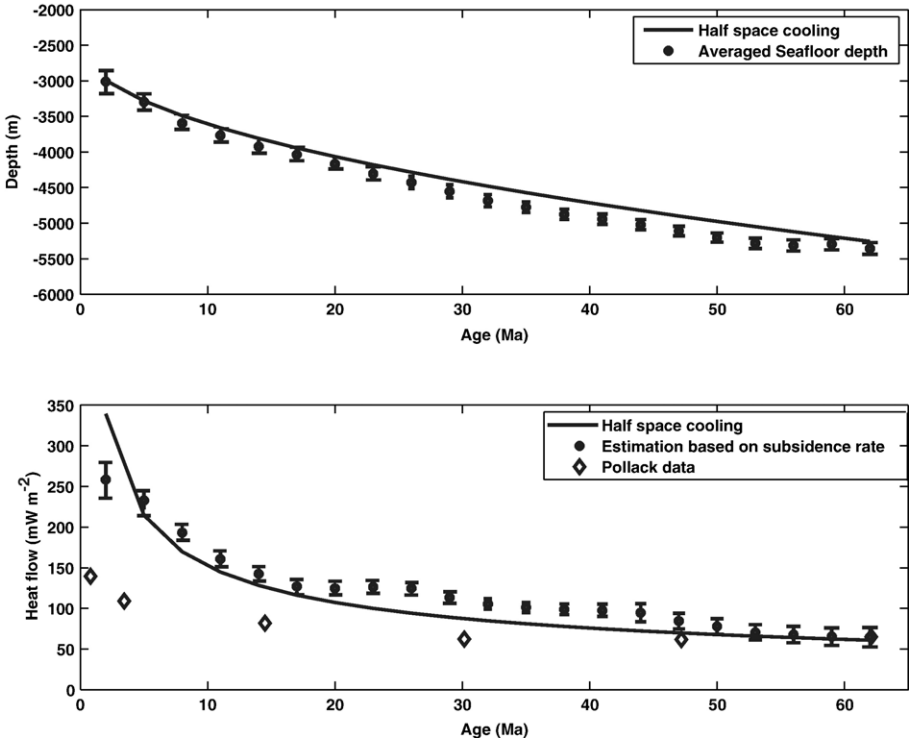

Fig. 2. (Top) Seafloor depth versus age of mid-Atlantic compared with prediction of half-space cooling model $d = 2500 + 350\sqrt{t}$. (Bottom) Heat flow of mid-Atlantic inferred from subsidence rate (Eq. (8)) compared with conductive heat flow measurements (Pollack et al., 1993) and half-space cooling model $q = 480/\sqrt{t}$. A constant heat flow of 38 mW m^{-2} was added to the estimated heat flow to account for the unobserved basal heat input Doin and Fleitout (1996). This new estimate is consistent with the half-space cooling model and inconsistent with the conductive measurements.

Fig. 3 (top) along with a surface heat flow based on the half space cooling model (Fig. 3, bottom). There is good qualitative agreement although the estimated heat flow still has considerable spatial variation even after low-pass filtering. Some of the large positive and negative spatial variations in heat flow are associated with topographic features that are Airy compensated. Consider a local bathymetric high; the gradient of the topography in the direction of increasing age will be sharply positive on the younger side and sharply negative on the older side. If the base level around the feature is the same on both sides and the fossil spreading rate is also the same, the false positive and negative estimated heat flow will cancel. We could attempt to mask these areas of anomalous depth; however, this cancellation effect will results in an overall unbiased estimate of heat flow. A similar argument does not apply to recovery of seafloor depth versus age because seamounts and plateaus can only make the depth shallower (thicker crust) and there is no compensating crustal thinning mechanism. This is why it is critical to remove seamounts and plateaus prior to analysis of depth versus age (Hillier and Watts, 2005). There are also spatial variations in heat flow apparently associated with ridge jumps and fossil microplates. This is to be expected because the age gradient can be discontinuous leading to small values in the denominator of the scalar subsidence rate.

As in the case of the mid-Atlantic Ridge, we average the depth and heat flow data into 3 Ma age bins between 0 and 66 Ma as shown in Fig. 4. The depth versus age data show progressive disagreement with the theoretical curve. We believe this is mostly a depth bias caused by seamounts and plateaus, which become more prominent on 40–60 Ma seafloor. Nevertheless the fit is good for seafloor with age less than 30 Ma.

Heat flow estimated from scalar subsidence rate shows excellent agreement with the half-space cooling model when a basal heat flux of 38 mW m^{-2} is added (Fig. 4, bottom). This basal heat flux was adjusted to match the measured conductive heat flow at 41 and 62 Ma (Pollack et al., 1993) and it agrees with the value proposed by Doin and Fleitout (1996). As in the case of the mid-Atlantic ridge, there is disagreement in the first age bin where we have been unable to estimate subsidence rate within 20 km of the ridge axis. The

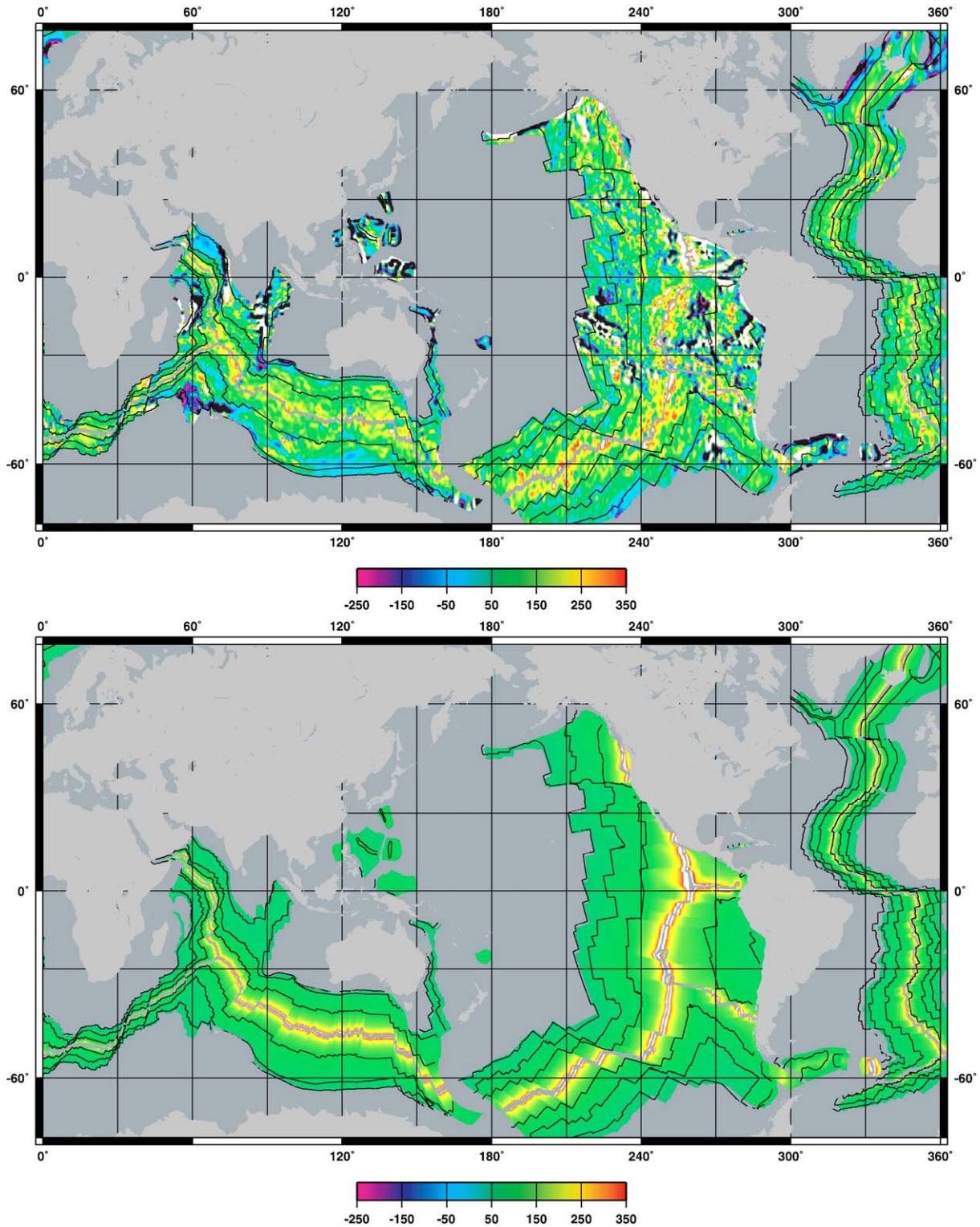

Fig. 3. (Top) Global heat flow based on subsidence rate (38 mW m^{-2} basal heat flow was added). (Bottom) Global heat flow based on space cooling model, $q = 480/\sqrt{t}$.

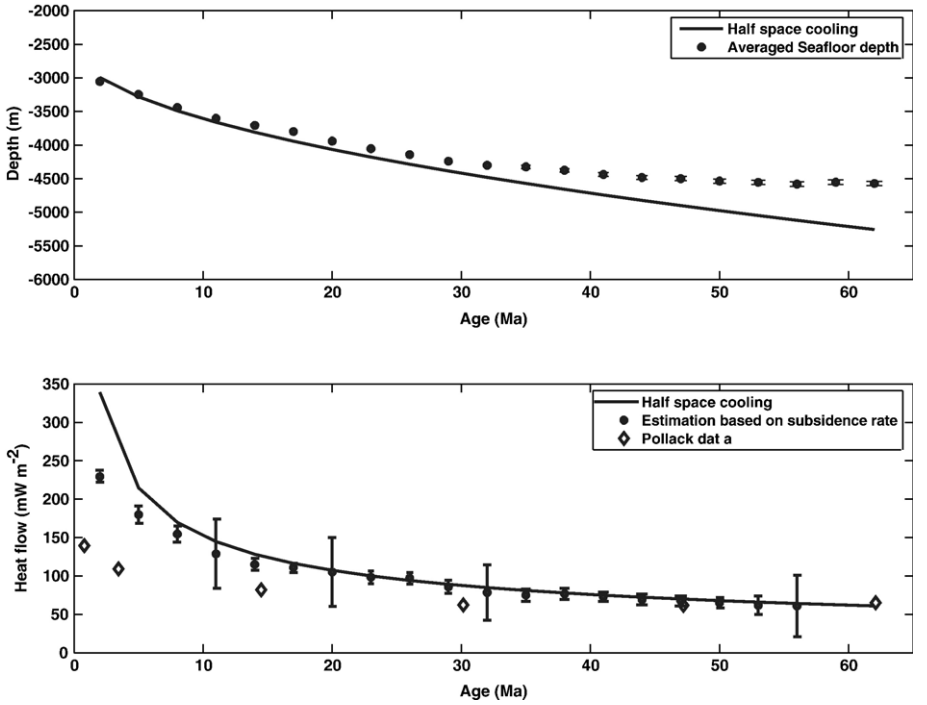

Fig. 4. (Top) Global seafloor depth versus age compared with prediction of half-space cooling model $d = 2500 + 350\sqrt{t}$. (Bottom) Global heat flow inferred from subsidence rate (Eq. (9)) with 38 mW m^{-2} basal heat flux added compared with conductive heat flow measurements (Pollack et al., 1993) and half-space cooling model $q = 480/\sqrt{t}$.

agreement is remarkably good between 6 and 66 Ma. The agreement would be poor if a basal heat flux was not added suggesting this is required, at least for ages greater than 40 Ma where measured conductive heat flow approaches the total heat flow.

5. Heat output of Cenozoic seafloor and the heat output of the Earth

Using our new estimates of surface minus basal heat flow we can estimate the global heat output of the Cenozoic seafloor. A first approach is to integrate our surface minus basal heat flow (plus 38 mW m^{-2}) from 3 to 66 Ma. This results in a total of 14.4 TW resulting in a global heat output of 37.6 TW. This estimate may be a lower bound because we are missing two contributions: we cannot estimate the heat flow within 20 km of the ridge axes, and we do not estimate heat flow in the Arctic ocean where depth and age are poorly constrained. Indeed we show next that these contributions are 5.1 TW.

A second approach to estimating Cenozoic heat output is based on our good fit to the half-space cooling (HSC) model (Fig. 4, bottom). If we assume the HSC model is correct and use the new age grid to estimate the total we arrive at an estimate of 20.4 TW in agreement with Pollack et al. (1993). The results are shown in Fig. 5 and numerical values are provided in Table 1. The upper plot is the area of seafloor divided into 3 Ma age bins from 0 to 66 Ma. The calculation of this area versus age relation out to 180 Ma approximately follows a linear decrease as proposed by Parsons (1982). The heat flow in each age bin times the area of the bin is shown in Fig. 5 (middle) where the theoretical heat is integrated over the age range t_1 to t_2 is

$$\overline{q}(\overline{t}) = \frac{1}{t_2 - t_1}\int_{t_1}^{t_2} Ct^{-1/2}dt = \frac{2C}{t_2 - t_1}\left(t_2^{1/2} - t_1^{1/2}\right) \qquad (9)$$

where C (480 mW m^{-2} $Ma^{-1/2}$) is the coefficient of the HSC model (Pollack et al., 1993). Note that 5 TW of the global heat flow is produced in the first 3 Ma (Fig. 5, middle). Since this is the age range where we are unable to estimate heat flow, our integrated estimate will be ~5 TW too low. The lower plot in Fig. 5 shows the cumulative sum of the oceanic heat flow from 0 to 66 Ma. Again, the first age bin contributes 5 TW and the remainder 15.4 TW for a total of 20.4 TW in agreement with previous estimates. It is interesting to note that Pollack et al. (1993) arrive at the same value but use a

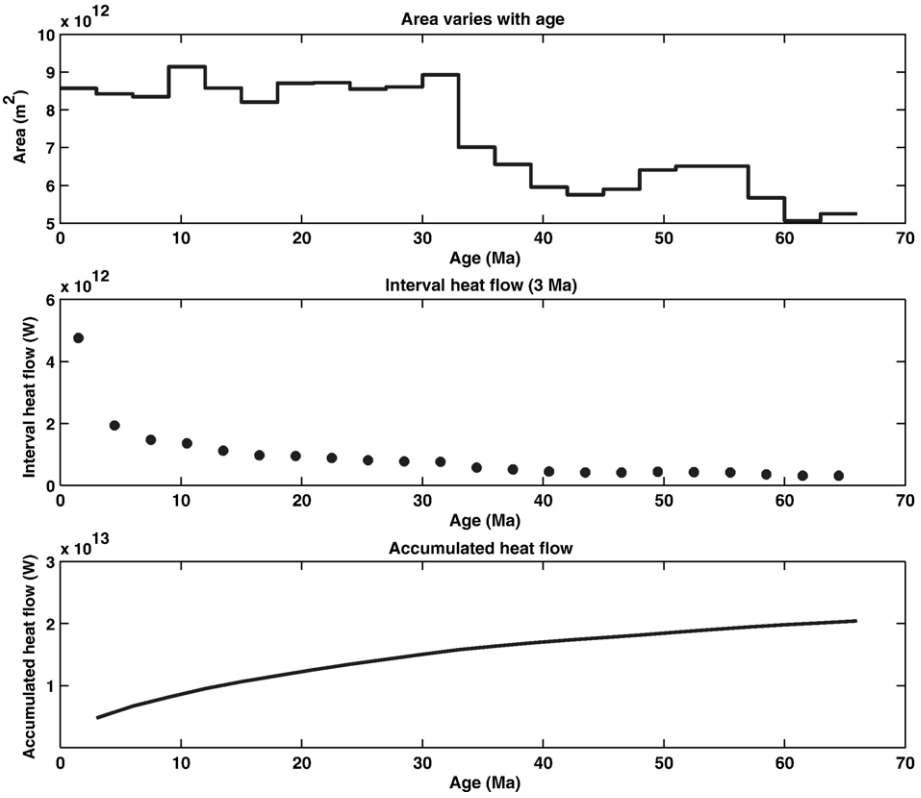

Fig. 5. Global oceanic heat flow from 0 to 66 Ma crust based on HSC model. (Top) Seafloor area versus age in 3 Ma bins based on the age grid of Mueller et al. (1997). (Middle) Total heat flow in for each age bins is the product of the integrated model heat flux (Eq. (9)) times the area of seafloor. The first age bin has 5 TW. (bottom) Age-integrated heat flow provides a total of 20.4 TW at 66 Ma.

model with a higher overall heat flow of $q = 510/\sqrt{t}$. We have used a lower value of 480 for the heat flow coefficient so we suggest that the more complete age grid has provided an increase in global heat flow to offset the lower heat flow coefficient.

Table 1
Cenozoic and global heat flow totals

Model		Q (TW)		Q_T (TW)
α (10^{-5} °C^{-1})	q_b (W m^{-2})	0–66	3–66	Global
2.9	28.9	–	15.4	44.1
3.5	**35.2**	–	**14.4**	**43.1**
3.85	38.0	–	14.0	42.7
4.2	40.0	–	13.5	42.2
7.0	50.2	–	12.0	35.6 (note the 0–3 Ma HSC is not included)
HSC, $q(t) = 960\frac{\sqrt{t_2}-\sqrt{t_1}}{t_2-t_1}$				
Lat. −70° to 90°		20.4	15.5	44.0
Lat. −70° to 70°		20.14	15.3	43.7

Global heat Q_T is the sum of integrated contribution (3–66 Ma), the 5.1 estimated from HSC (0–3 Ma), and the 23.6 from continents and older oceans (Pollack et al., 1993). Values in bold are the most possible results we proposed.

The agreement between our estimates and the half-space cooling model suggests that the total heat output of the Earth is close to the 44 TW value. However, there are two uncertainties in our calculations. First we have added an unknown basal heat flux of 38.0 mW m^{-2}. All lithospheric cooling models require some basal heat flux to explain the flattening of the depth vs. age relation in combination with the relatively high heat flow observed on very old seafloor of 50 mW m^{-2} (Stein and Abbott, 1991). If we remove this basal heat contribution, we obtain an integrated heat flow of 13.5 TW resulting in a global output of only 37.1 TW. The second uncertainty is our estimate of the heat capacity and the thermal expansion coefficient. The temperature-averaged heat capacity has a rather narrow range between 1094 and 1124 J kg^{-1} °C^{-1} depending on the dominant minerals (Fig. 6, top). However, the temperature-averaged thermal expansion coefficient has a much larger range between 2.9 and 4.2×10^{-5} °C^{-1} (Fig. 6, bottom).

Given these uncertainties in thermal expansion coefficient and basal heat flux we can only place bounds on the Cenozoic heat output (Table 1 and Fig. 7). The possible range of heat capacity is small so we set this

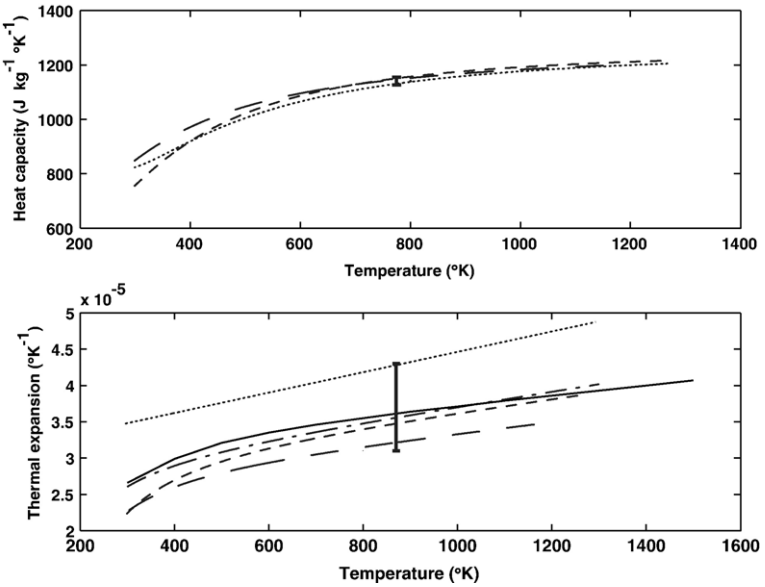

Fig. 6. (Top) Heat capacity of candidate minerals in the lithosphere (Fei and Saxena, 1987). Long-dashed: olivine; short-dashed: spinel; dots: clinopyroxene. The range of temperature-integrated heat capacity of 1094 to 1124 J kg^{-1} °C^{-1} is illustrated by the vertical bar. (Bottom) Thermal expansion coefficient for olivine from different experiments involving slightly different minerals. Long-dashed: Mg_2SiO_4, (Suzuki, 1975); dots: Mg_2SiO_4, (Hazen, 1976); short-dashed: Mg_2SiO_4, (Matsui and Manghnani, 1985); mix-dashed: Mg_2SiO_4, (Kajiyoshi, 1986); solid: $(Mg.9Fe.1)_2SiO_4$, (Anderson and Isaak, 1995). The range of temperature-integrated thermal expansion coefficient of 3.0 to 4.2×10^{-5} °C^{-1} is illustrated by the vertical bar.

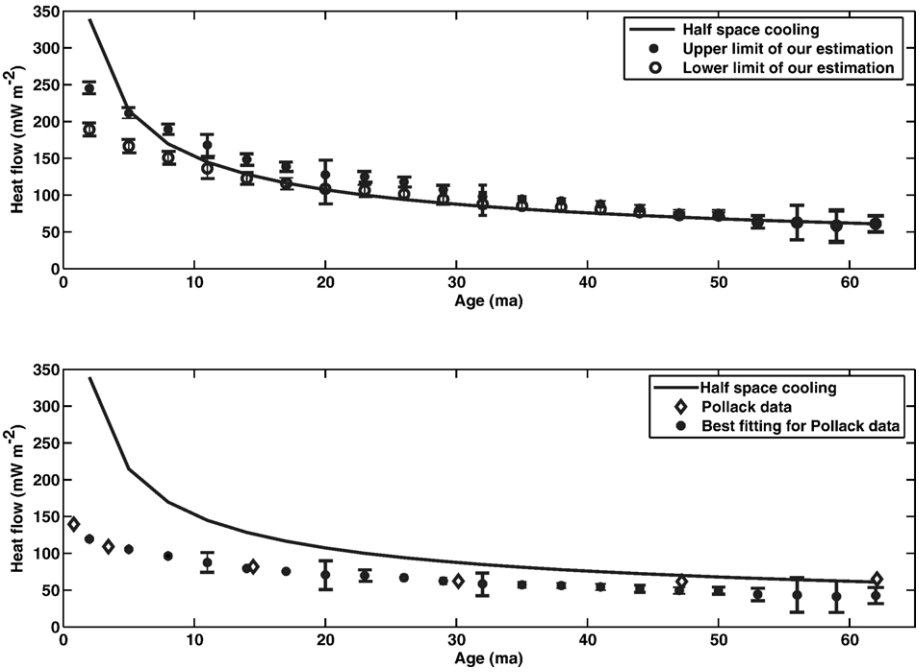

Fig. 7. (Top) The lower and upper bounds on estimated heat flow compared with the HSC model $q = 480/\sqrt{t}$ using thermal expansion coefficient of 2.9 and 4.2×10^{-5} °C^{-1}, respectively. (Bottom) Our estimates of heat flow match the data of Pollack et al., 1993 but only if an unrealistically high value of thermal expansion coefficient is used (7.0×10^{-5} °C^{-1}).

value to 1124 J kg^{-1} $°C^{-1}$. Next we vary the thermal expansion coefficient over the possible range of 2.9 to 4.2×10^{-5} $°C^{-1}$ and calculate the surface minus basal heat flux. Finally, we estimate the basal heat flux by varying this parameter so the estimated heat flow in the 45 to 66 Ma age range matches the values of the HSC model. We use the HSC model rather than the two estimates from Pollack et al. (1993) because the HSC model also provides a good fit to heat flow data on older seafloor (66–120 Ma). The results (Table 1 and Fig. 7 (top)) provide integrated heat flow (3–66 Ma) ranging between 13.5 and 15.4 TW. To this we add the 5.1 TW that is predicted from the HSC model on young seafloor (0–3) to obtain the Cenozoic heat output and ultimately the global estimate range based on the non-Cenozoic estimates from Pollack et al. (1993). The global heat flux ranges between 42.2 and 44.1 TW; a likely thermal expansion of 3.5×10^{-5} $°C^{-1}$ provides a global heat estimate of 43.1 TW.

The main weakness of our method is that it relies on the HSC cooling model to estimate the 5-TW contribution to the heat flow over the spreading ridges (0–3 Ma). Even if there were no heat flow from ridges, Cenozoic heat flow would still be between 37.1 and 39 TW, greater than the global estimate of Hofmeister and Criss (2005). Of course, high heat flow at spreading ridges is well documented by dozens of studies (e.g., Von Herzen et al., 2005), so global heat output must be greater than 37.1–39 TW. Another weakness of our method is that we rely on a poorly known value of the lithospheric-averaged thermal expansion coefficient. It is possible to match the Pollack et al. (1993) conductive heat flow data with subsidence rate data although this requires an unrealistically high thermal expansion coefficient of 7.0×10^{-5} $°C^{-1}$ (Fig. 7, bottom). The highest thermal expansion of any naturally occurring mineral is 5.1×10^{-5} $°C^{-1}$ (Anderson and Isaak, 1995) so this situation is also not possible.

6. Conclusion

Conductive heat flow measurements over young oceanic lithosphere are significantly less than the prediction of lithospheric cooling models. This has led to a debate concerning the global heat output of the Earth. Model-based estimates of oceanic heat flux provide an upper bound of 42–44 TW (Sclater et al., 1980; Pollack et al., 1993) while measurement-based estimates (conductive only) provide a lower bound of ~35 TW (Hofmeister and Criss, 2005). Note we have not addressed the 4 TW of difference in continental heat flow between the estimates of Pollack et al. (1993) and Hofmeister and Criss (2005). The overall elevation of the global ridge system, relative to the deep ocean basins, provides an estimate of the total heat content of the lithosphere. We re-derive an expression relating heat flow to local scalar subsidence rate and show that this relationship is independent of the vertical heat transport mechanism. The derivation relies only on conservation of energy, thermal expansion, and local isostasy. Heat flow out of the top of the plate minus the heat flow into the bottom of the plate is proportional to the measured subsidence rate times the heat capacity divided by the thermal expansion coefficient.

We develop a method of estimating scalar subsidence rate directly from depth and age gradients. Since the age gradient is discontinuous across plate boundaries, the method fails over very young seafloor. Additionally, the model assumes local isostatic balance so the flexure and dynamic topography within 20 km of the ridge axis must also be avoided. This zone includes the first 3 Ma of seafloor where half-space cooling models predict that 5 TW of power escapes. Therefore our method omits the contribution from 0 to 3 Ma seafloor. The estimates of the heat flow difference between the upper and lower surfaces of the plate over the 3–66 Ma age range are robust.

We compute global maps of surface minus basal heat flow that show qualitative agreement with heat flow based on the inverse square root of age relation. Averaging these estimates over 3 Ma age bins shows excellent agreement with the heat flow based on the Parsons and Sclater (1977) cooling model if a basal heat flux of 38 mW m^{-2} is added. This extra contribution is needed to fit observed conductive heat flow in the 45–66 Ma age range. Our results are 9 TW larger than the observations of conductive heat flow for ages less than 40 Ma suggesting that another heat transport mechanism must operate (e.g. hydrothermal circulation). We evaluated uncertainties in Earth's lithospheric heat output based on uncertainties in the temperature-averaged heat capacity and thermal expansion coefficient, but these are much smaller than the difference between previous global estimates (42–44 TW) and the more recent estimate by Hofmeister and Criss (2005) (35 TW). Our results based on experimentally derived values of heat capacity and thermal expansion coefficient suggest global heat output of 43 TW, consistent with most earlier estimates. Thus we conclude that the Hofmeister and Criss (2005) estimate is low by ~8 TW as a result of assuming that the hydrothermal heat flux from oceanic lithosphere is much smaller than it actually is. We also conclude that observed differences in the elevation of the ridges and ridge flanks are a first-order

measure of the heat loss of the cooling lithosphere, and that the total oceanic heat flow is in accordance with conductive cooling models.

Acknowledgements

We thank the editor, Hans Thybo and reviewers, Andrew Fisher and an anonymous reviewer for their excellent suggestions on improving the paper. The paper benefited from discussions with Norm Sleep and Guy Masters. This research was supported by NASA Solid Earth and Natural Hazards Program (NAG-5-13673) and the National Science Foundation, Marine Geology and Geophysics Program (OCE 0326707).

References

Anderson, O.L., Hobart, M.A., 1976. The relation between heat flow, sediment thickness, and age in the eastern Pacific. J. Geophys. Res. 81, 2968–2989.

Anderson, O.L., Isaak, D.G., 1995. Elastic constants of mantle minerals at high temperature. Mineral Physics and Crystallography, a handbook of Physical Constants, AGU reference shelf, vol. 2, pp. 64–97.

Cochran, J.R., 1979. An analysis of isostaty in the world's oceans: 2. Midocean ridge crests. J. Geophys. Res. 84, 4713–4729.

Cochran, J.R., Buck, W.R., 2001. Near-axis subsidence rates, hydrothermal circulation, and thermal structure of the mid-ocean ridge crests. J. Geophys. Res. 106, 19233–19258.

Davis, E.E., Lister, C.R.B., 1974. Fundamentals of ridge crest topography. Earth Planet. Sci. Lett. 21 (4), 405–413.

Doin, M.P., Fleitout, L., 1996. Thermal evolution of the oceanic lithosphere: an alternative view. Earth Planet. Sci. Lett. 142, 121–136.

Fei, Y., Saxena, S.K., 1987. An equation for the heat capacity of solids. Geochim. Cosmochim. Acta 51, 251–254.

Hazen, R.M., 1976. Effects of temperature and pressure on the crystal structure of forsterite. Am. Mineral 61, 1280–1293.

Hillier, J.K., Watts, A.B., 2005. Relationship between depth and age in the North Pacific Ocean. J. Geophys. Res. 110, B02405.

Hofmeister, A.M., Criss, R.E., 2005. Earth's heat flux revised and linked to chemistry. Tectonophysics 395, 159–177.

Kajiyoshi, K., 1986. High temperature equation of state for mantle minerals and their anharmonic properties. Ph.D. Thesis, Okayama Univ.

Lister, C.R.B., 1972. On the thermal balance of a mid-ocean ridge. Geophys. J.R. Astron. Soc. 26, 515–535.

Matsui, T., Manghnani, M.H., 1985. Thermal expansion of single-crystal forsterite to 1023 K by Fizeau interferometry. Phys. Chem. Miner. 12, 201–210.

McKenzie, D.P., 1967. Some remarks on heat flow and gravity anomalies. J. Geophys. Res. 72, 6261–6273.

Mueller, R.D., Roest, W.R., Royer, J.-Y., Gahagan, L.M., Sclater, J.G., 1997. Digital isochrons of the world's ocean floor. J. Geophys. Res. 102, 3211–3214.

Oldenburg, D.W., 1975. A physical model for the creation of the lithosphere. Geophys. J. R. Astron. Soc. 43, 425–451.

Parsons, B., 1982. Causes and consequences of the relation between area and age of the ocean floor. J. Geophys. Res. 87 (B1), 289–302.

Parsons, B., McKenzie, D., 1978. Mantle convection and the thermal structure of the plates. J. Geophys. Res. 83, 4485–4496.

Parsons, B., Sclater, J.G., 1977. An analysis of the variation of ocean floor bathymetry and heat flow with age. J. Geophys. Res. 82, 803–827.

Pollack, H.N., Hurter, S.J., Johnson, J.R., 1993. Heat flow from the Earth's interior: analysis of the global data set. Rev. Geophys. 31, 267–280.

Renkin, M.G., Sclater, J.G., 1988. Depth and age in the North Pacific. J. Geophys. Res. 93 (B4), 2919–2935.

Sandwell, D.T., Poehls, K.A., 1980. A compensation mechanism for the central pacific. J. Geophys. Res. 85, 3751–3758.

Sclater, J.G., Jaupart, C., Galson, D., 1980. The heat flow through oceanic and continental crust and the heat loss of the earth. Rev. Geophys. Space Phys. 18, 269–311.

Sleep, N.H., Wolery, T.J., 1978. Egress of hot water from midocean ridge hydrothermal systems: some thermal constraints. J. Geophys. Res. 83, 5913–5822.

Smith, W.H., Sandwell, D.T., 1997. Global sea floor topography from satellite altimetry and ship depth soundings. Science 277 (5334), 1956–1962.

Stein, C.A., Abbott, D., 1991. Heat flow constraints on the South Pacific Superswell. J. Geophys. Res. 96, 16083–16100.

Stein, C.A., Stein, S.A., 1992. A model for the global variation in oceanic depth and heat flow with lithospheric age. Nature 359, 123–128.

Stein, C.A., Stein, S.A., 1994. Constraints on hydrothermal heat flux through the oceanic lithosphere from global heat flow. J. Geophys. Res. 88, 3081–3095.

Suzuki, I., 1975. Thermal expansion of periclase and olivine and their anharmonic properties. J. Phys. Earth 23, 145–159.

Von Herzen, R., Davis, E.E., Fisher, A.T., Stein, C., Pollack, H.N., 2005. Comment on "Earth's heat flux revised and linked to chemistry" by A.M. Hofmeister and R.E. Chris. Tectonophysics 409, 193–198.

Williams, D.L., Von Herzen, R.P., Sclater, J.G., Anderson, R.R., 1974. The Galapagos spreading centre: lithospheric cooling and hydrothermal circulation. Geophys. J. R. Astron. Soc. 38, 587–608.